# Structural basis for conductance by the archaeal aquaporin AqpM at 1.68 Å

John K. Lee*, David Kozono†‡, Jonathan Remis*, Yoshichika Kitagawa§, Peter Agre†¶, and Robert M. Stroud*‖

*Macromolecular Structure Group, Department of Biochemistry and Biophysics, University of California, S-412C Genentech Hall, 600 16th Street, San Francisco, CA 94143-2240; †Department of Biological Chemistry and Medicine, The Johns Hopkins University School of Medicine, Baltimore, MD 21205-2185; and §Genetic Engineering, Graduate School of Bioresource, Akita Prefectural University, Shimoshinjo, Akita 010-0195, Japan

To explore the structural basis of the unique selectivity spectrum and conductance of the transmembrane channel protein AqpM from the archaeon *Methanothermobacter marburgensis*, we determined the structure of AqpM to 1.68-Å resolution by x-ray crystallography. The structure establishes AqpM as being in a unique subdivision between the two major subdivisions of aquaporins, the water-selective aquaporins, and the water-plus-glycerol-conducting aquaglyceroporins. In AqpM, isoleucine replaces a key histidine residue found in the lumen of water channels, which becomes a glycine residue in aquaglyceroporins. As a result of this and other side-chain substituents in the walls of the channel, the channel is intermediate in size and exhibits differentially tuned electrostatics when compared with the other subfamilies.

integral membrane protein | x-ray crystallography | water channel | gas

**A**quaporins are a large family of transmembrane channel proteins that facilitate the passive, but highly selective, movement of water, small neutral alditols, including glycerol, or $CO_2$ across cell membranes (1). These channels are found throughout all domains of life and are fundamental elements in the osmoregulation of many organisms. The selectivity and biophysical characteristics of several aquaporins have been described through atomic resolution structures. The atomic resolution structures of aquaporins GlpF (2), Aqp1 (3, 4), AqpZ (5), Aqp0 (6, 7), and now most recently, AqpM, show high similarity in their tertiary structures. However, despite the similarity in topology and quaternary structure across the family, *in vivo* and *in vitro* water and glycerol conductance assays (8–10) have shown that each member exhibits unique conductance rates and displays selectivity spectra that extend to the selective permeation of small neutral molecules that include glycerol, urea, and $CO_2$.

The structural congruity that spans this family points to the side-chain variations in the channels as the main basis for the divergence in the selectivity and conductance rates between different aquaporins. For example, the crystal structures revealed the integral role of the extended loop that leads into the central plane of the membrane bilayer from each side of the membrane to the conserved -NPA- motifs that initiate the half-membrane spanning helices. These features are a signature for the entire family. Each of these loops provides a ladder of four carbonyl oxygens from successive amino acids in the sequence that are presented into the lumen of the channel. Forming a helical set of hydrogen-bond acceptors from one side to the other along the axis of the channel, they generate a ladder of hydrogen-bond-accepting groups spaced ≈2.8 Å apart in distance through the channel. They determine a key element of the chemical environment for the coordination and conductance of the permeants through the lumen of the channel. Also, the side chains that form the selectivity filter influence the electrostatics and diameter of the channel at its narrowest juncture (2) and separate the water-selective aquaporins such as Aqp1 and AqpZ from the glycerol-conducting subfamily (aquaglyceropor-

ins) that includes the *Escherichia coli* glycerol channel GlpF and human aquaporins 3, 7, 9, and 10.

The discovery and characterization of AqpM (11) from the methanogenic archaeon *Methanothermobacter marburgensis* as an aquaporin confirmed the presence of aquaporins in archaea (12). Because of the absence of any other aquaporins in the genome of *Methanothermobacter marburgensis*, the primary function of AqpM is most likely to facilitate the movement of water across the plasma membrane in response to osmotic gradients of its environment. *In vitro* and *in vivo* conductance assays verified that AqpM is indeed a water-conducting channel (13), albeit with a lower permeability rate for water ($P_f$) than other water-selective aquaporins such as AqpZ [$P_f$(AqpM) = 57 ± 4 μm/s (13); $P_f$(AqpZ) = 330 μm/s (8)]. AqpM has also been observed to conduct glycerol at a low rate, but in *Methanothermobacter marburgensis*, which relies on $CO_2$ as its sole carbon source, this function may prove to be biologically irrelevant (13).

Because of the high similarity in the structures of most aquaporins, several unusual qualities of AqpM provide awareness for deciphering the mechanism of selectivity and conductance by aquaporins. First, an isoleucine residue replaces the highly conserved histidine residue located in the selectivity filter of water-selective aquaporins. This difference may represent an adaptation specific for function in addition to the conduction of water. In support of this speculation, initial studies indicate the conductance of $CO_2$ by AqpM (Y.K., unpublished data). The identification of certain aquaporins as $CO_2$ channels has been a topic of some interest and controversy (14, 15), although recent studies have shown the conductance of $CO_2$ by bovine Aqp1 (16) and tobacco aquaporin NtAQP1 (10). Notably, these two aquaporins are highly expressed in membranes involved in the high traffic of $CO_2$, namely the membranes of red blood cells and plant leaves. The demand for specific and efficient conductance of this gas by certain cells and the characterization of aquaporins with this functional capacity supports the possibility that aquaporins may be this elusive gas channel.

Here, we report the atomic structure of AqpM to 1.68-Å resolution. Based on this structure, we elaborate the relationships between the structure, rate of conductance, and selectivity by this transmembrane channel protein for water and glycerol. The structure of AqpM supports the role of the channel vestibules in preselecting the permeants and beginning the energetically unfavorable process of stripping the hydration shell from around the molecule before it is transported into and through the narrow portion of the channel.

## Materials and Methods

**Expression of 10-His-Tagged AqpM and Purification.** Recombinant AqpM was expressed and purified as described (13) with some modifications. The cells were lysed by subjecting them to three microfluidizer cycles (15,000–18,000 pounds per square inch) at 4°C. Cellular debris and unlysed cells were pelleted by centrifugation at $8,000 \times g$ for 20 min. The membrane was recovered by ultracentrifugation at $138,000 \times g$ for 1 h. The protein was solubilized from membrane with ≈30 ml of solubilization buffer [50 mM Tris, pH 7.4/10% (vol/vol) glycerol/300 mM NaCl/1 mM PMSF] by slowly adding octyl-$\beta$-D-glucoside (OG) (Anatrace, Maumee, OH) to a final detergent concentration of 5.0% (vol/vol). The solubilization mixture was incubated at 4°C for 3 h while stirring. The insoluble material was pelleted by ultracentrifugation at $138,000 \times g$, and the soluble fraction was mixed with 3 ml of $Co^{2+}$-Sepharose [equilibrated with 50 mM Tris, pH 7.4, 300 mM NaCl, 1.2% OG, 10% glycerol (vol/vol), and 1 mM PMSF] and incubated with gentle agitation at 4°C overnight. The resin was then packed in a chromatography column and washed with 50 ml of buffer (1.2% OG/50 mM Tris, pH 7.4/10% glycerol/50 mM imidazole/300 mM NaCl) to remove nonspecifically bound materials. Co-nitrilotriacetic acid-agarose-bound material was eluted with elution buffer (1.2% OG/50 mM Tris, pH 7.4/10% glycerol/300 mM NaCl/300 mM imidazole). The eluted sample was concentrated and purified by size-exclusion chromatography (1.2% OG/50 mM Hepes, pH 7.4/100 mM NaCl). The sample was digested with Factor Xa (Novagen) for 12 h at 22°C to remove the affinity tag and was further purified by size-exclusion chromatography. The sample was concentrated by using Amicon Ultra centrifugal concentrators to a final concentration of ≈10 mg/ml for crystallization trials.

**Crystallization.** Initial crystal conditions were screened by using Nextal PEG Screen (Nextal Biotechnologies, Montreal) for hanging drop vapor diffusion experiments (1-$\mu$l sample + 1-$\mu$l well solution) at 22°C. Small crystals (<50 $\mu$m along the long axis) were seen in conditions containing ≈25% polyethylene glycol (PEG) 2000 MME, 3000, and 4000 at pH 7.5–9.0. Conditions were optimized, and crystals with good-quality diffraction appeared in 2–3 days and matured to full size in ≈2 weeks (Tris, pH 9.0/100 mM NaCl/20% PEG 4000/10% glycerol). The best diffracting crystal form is tetragonal in morphology and ≈200–300 $\mu$m along the long $c$ axis. Phase separation in the crystal drop was a common feature in many crystallization conditions. However, many crystals grew in the detergent-rich phase of the drop, and a crystal used to determine the structure to 2.3-Å resolution grew from the center of one such drop. To avoid the phase separation, crystallization trials were set with protein samples concentrated to ≈10 mg/ml and dialyzed for 3 days. Conditions set up with these dialyzed samples had no phase separation in conditions up to 27% PEG 4000. The highest diffracting crystal grew in ≈2 weeks in conditions similar to that of the crystals that grew in the detergent-rich phase (Tris, pH 8.5/200 mM $MgCl_2$/23% PEG 4000/10% glycerol).

**X-Ray Diffraction and Data Processing.** Diffraction data of single crystals frozen in liquid nitrogen were collected under cryoconditions at Beamline 8.3.1 (Lawrence Berkeley National Laboratory, Berkeley, CA) on a Quantum-4 CCD Detector (Area Detector Systems, Poway, CA). Data were indexed and scaled by using DENZO/SCALEPACK (17). The molecular replacement solution was found by using the transmembrane helices of AqpZ as a search model. Molecular replacement and subsequent refinement calculations were performed with CNS (18). The model was built by using MOLOC (19). The final statistics are listed in Table 1.

### Table 1. Data collection and refinement statistics

| Crystal data | | |
|---|---|---|
| Space group | *I*4 | *I*4 |
| Unit cell, Å | $a = 93.9$ | $a = 88.5$ |
| | $c = 77.7$ | $c = 79.9$ |
| X-ray data collection statistics | | |
| Wavelength, Å | 1.11 | 1.11 |
| Resolution, Å | 60–2.3 | 60–1.68 |
| Total reflections | 96,055 | 322,170 |
| Unique reflections | 15,512 | 34,033 |
| Redundancy (last shell) | 2.1 | 18.6 (7.9) |
| Completeness (last shell), % | 95.4 (86.0) | 96.8 (83.2) |
| $R_{sym}$, % | 8.7 | 7.7 |
| $I/\sigma$ (last shell) | 13 (2.0) | 26.1 (3.3) |
| Crystallographic refinement statistics | | |
| Resolution, Å | 40–2.3 | 40–1.68 |
| Reflections in working set | 14,387 | 34,031 |
| Reflections in test set (5.0%) | 1,440 (10%) | 1,665 (5%) |
| $R_{cryst}$, % | 18.8% | 18.4% |
| $R_{free}$, % | 22.6% | 19.3% |
| RMSD bonds, Å | 0.007 | 0.008 |
| RMSD angles, ° | 1.06 | 1.11 |
| Average $B$ factors, Å$^2$ | 56.6 | 17.1 |

RMSD is the rms deviation from ideal geometry. $R_{sym} = \Sigma_{hkl}\Sigma_i \mid I_{hkl,i}\langle|_{hkl,i}|\rangle|/\Sigma_{hkl}\Sigma_i/| \mid |_{hkl,i} \mid$, where $\langle|_{hkl,i}|\rangle$ is the average intensity of the multiple hkl observations for symmetry-related reflections. $R_{cryst} = \Sigma \mid F_{obs} - F_{calc} \mid \Sigma F_{obs}$, where $F_{obs}$ and $F_{calc}$ are observed and calculated structure factors, $R_{free}$ is calculated from a randomly chosen 5% or 10% of reflections, and $R_{cryst}$ is calculated over the remaining reflections.

## Results

**Structure of AqpM.** The structure of AqpM was initially determined to 2.3-Å resolution by x-ray crystallography with a single crystal of AqpM, which gave anisotropic diffraction to 2.1-Å resolution in the best direction. The initial phases and the solution of the structure were obtained by molecular replacement with the core helices of AqpZ as the search model. The final refined structure is based on data to 1.68-Å resolution, refined to $R_{cryst}$ of 19.2% and $R_{free}$ of 20.0% (Table 1).

As in the other aquaporin structures reported to date, AqpM crystallizes as a homotetramer with each monomer forming an independent transmembrane channel (Fig. 1). The asymmetric unit of the crystal unit cell is one monomer with the 4-fold tetrameric axis coincident with the crystallographic 4-fold axis of the crystal. The structure shows 245 of the 246 residues of the primary sequence; only the carboxyl-terminal glutamate residue (E246) is not defined in the structure. Two octyl-$\beta$-D-glucopyranoside molecules are found associated with each monomer in the 2.3-Å resolution structure whereas they are absent in the high-resolution structure, and four water and three glycerol molecules are found coordinated inside the channel.

AqpM follows the canonical aquaporin fold of a right-handed helical bundle consisting of six transmembrane (M1–M2, M4-M6, and M8) and two half-membrane spanning helices (M3 and M7) (Fig. 1*A*). Both amino and carboxyl termini are located at the cytoplasmic side of the membrane. One additional short helix, situated between helices M4 and M5, sits parallel to the plane of the membrane on the extracellular surface, similar to a short helix observed in the structure of AqpZ. The circular bundle of transmembrane helices generates the channel along its central axis, which is ≈27 Å long, averages ≈4 Å in diameter, and widens to conical vestibules at both ends. Additionally, helix M1 is extraordinarily long compared with its counterpart in other aquaporin structures, accounting for some of the structural variation between AqpM and other aquaporins. Loop A, which connects helices M1 and M2, is particularly large compared with
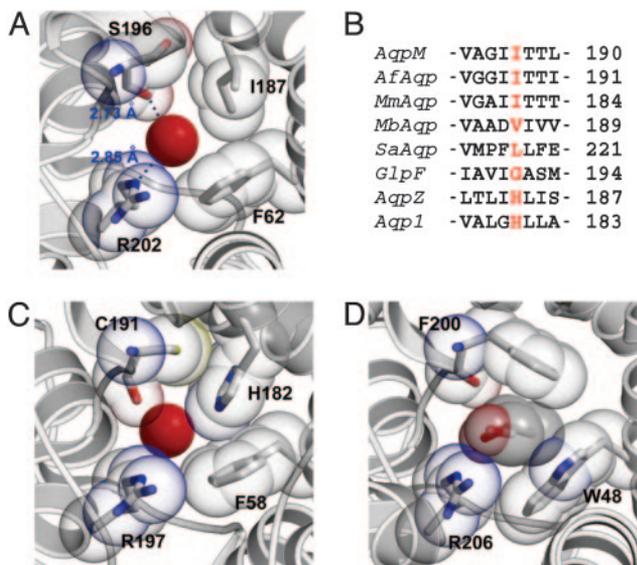
**Fig. 1.** Monomer and tetramer view of AqpM. (*A*) AqpM monomer viewed parallel to the plane of the membrane. The six transmembrane (M1–M2, M4–M6, and M8) and two half-membrane (M3 and M7) spanning helices are labeled M1–M8. The glycerol and water molecules found in the channel are represented as spheres. The two OG detergent molecules identified in the structure are represented as transparent spheres. The channel is readily identifiable by the line of water and glycerol molecules coordinated inside the channel. (*B*) The AqpM tetramer viewed down the 4-fold axis of the tetramer from the extracellular aspect of the membrane. Four residues that form the selectivity filter are shown in stick rendering. (*C*) Stereoview of the sigma-weighted 2 $F_o - F_c$ electron density at the selectivity filter. The map is contoured at 1.2 $\sigma$. The figure was made with MOLSCRIPT (25), RASTER3D (26), and PYMOL (27).

its equivalent in other aquaporins. This long loop provides a structural role in forming a part of the tetramer interface. It also folds to generate a hydrophobic pocket on the extracellular surface that is bound by glycerol and water molecules and is a part of the channel vestibule.

The differences between the low-resolution (2.3 Å) and high-resolution (1.68 Å) structures are minimal with a rms deviation of 0.17 Å between the two. However, differences exist in the location and presence of water, glycerol, and detergent molecules associated with the protein. The detergent molecules are only in the low-resolution structure. The location of water and glycerol molecules in the channel are also slightly different. The pore of the high-resolution structure is occupied almost exclusively by water molecules, with one glycerol molecule present at the -NPA- region of the channel. The low-resolution structure reveals four water molecules (HOH1–HOH4) and three glycerol molecules (G1–G3) lined up in single file along the channel, with each molecule hydrogen-bonded to its neighbor, while the main-chain carbonyl oxygens that line the channel provide hydrogen-bond acceptors for the permeant molecules (Fig. 2). Traveling from the extracellular side of the channel to the cytoplasmic side down the transmembrane axis of the channel, a glycerol (G1) molecule occupies the first position, at the mouth of the channel, stabilized by a hydrogen bond (2.67 Å) between the hydroxyl group of C2-OH and the main-chain carbonyl oxygen of G133(135) (all AqpM residue numbers are followed by GlpF numbering in parenthesis for reference). G1 is followed by three successive water molecules (HOH1, HOH2, and HOH3), located adjacent to the carbonyl oxygens of G195(198) (2.81 Å),

S196(199) (2.68 Å), and S197(200) (2.56 Å), respectively. HOH3 is followed by G2, which is adjacent to both the aquaporin canonical NPA motifs of helices M3 and M7. G2 is followed by



**Fig. 2.** AqpM channel architecture. Stereoview of the channel with potential hydrogen bonds to the waters (HOH1–H4) and glycerols (G1–G3) shown in gray dotted lines. Helices of M3 and M7 are rendered in cartoon representation, while the loop portion residues are represented as sticks. The main-chain carbonyl oxygens of the two loops form the conserved ladder-like structure of hydrogen-bond acceptors that line the channel. N82 and N199 are the asparagines that make up the canonical aquaporin NPA motifs.

**Fig. 3.** Aquaporin selectivity filters. (*A*) The residues of the selectivity filter of AqpM (R202, F62, S196, and I187) are depicted with the water molecule (HOH2) coordinated at the center of the filter. The potential hydrogen bonds from HOH2 to S196 and R202 are depicted as a blue dotted line. (*B*) The sequence alignment of six aquaporins. I187 from AqpM and corresponding residues in the other aquaporins are highlighted in the red box. In water-selective aquaporins, represented here by Aqp1 and AqpZ, a conserved histidine residue occupies this position. In aquaglyceroporins such as GlpF, a glycine residue occupies this position. Similar to AqpM, the two other archaeal aquaporins [*A. fulgidus* aquaporin (AfAqp) and *Methanosarcina barkeri* aquaporin (MbAqp)] possess aliphatic residues at this position. SaAqp, *S. acidocaldarius* aquaporin. MmAqp, *Methanococcus maripaludis* aquaporin. (*C* and *D*) The selectivity filters of Aqp1 (*C*) and GlpF (*D*) highlighting the similarity and differences between an aquaporin and aquaglyceroporin. A glycerol molecule is seen only in the selectivity filter of GlpF (*D*).

HOH4, which is stabilized by a hydrogen bond to the carbonyl oxygen of H80 (3.10 Å). Lastly, G3 occupies the cytoplasmic end of the channel.

The channel constricts to its narrowest point at the selectivity filter. The filter is formed by the side chains of R202(206), F62(48), and I187(191) and the carbonyl oxygen of S196(191) (Fig. 3*A*). The Nε of the guanidino group of R202(206) along with the carbonyl oxygen of S196(191) forms the hydrogen-bond donor and acceptor pair along half of the roughly circular filter (when viewed normal to the membrane plane), while the hydrophobic residues F62(48) and I187(191) form the other half. The topology of the selectivity filter is almost identical to that of other water-selective aquaporins, with the exception of I187(191), which replaces the highly conserved histidine residue (Fig. 3*B*). The arrangement of these residues constricts the diameter of the channel [all channel diameters cited were as calculated by the HOLE2 (20) program] to its minimum of 2.54 Å, 0.68 Å wider than that of the equivalent site in the water-specific Aqp1 (1.86 Å) (Fig. 3*C*) and 0.60 Å narrower than that of the aquaglyceroporin GlpF (3.14 Å) (Fig. 3*D*). Notably, this calculated diameter is similar to that of the diameter of a water molecule (2.8 Å) and presents good accommodation for the passage of water. Although the diameter calculation represents the largest spherical molecule that can pass through a roughly circular pore, this value presents a fairly good approximation even for the noncircular aquaporin channel because it represents the largest sphere that can pass through this pore.

Three highly ordered water molecules (HOH1–HOH13) are found at or near the selectivity filter in both the high- and low-resolution structures. HOH1 sits on the extracellular side of the selectivity filter and is hydrogen-bonded to the carbonyl oxygen of G195(190) (2.73 Å) and NH2 of R202(206) (2.85 Å). HOH2 is coordinated at the cytoplasmic side of the selectivity filter and is hydrogen-bonded to the Nε of R202(206) (2.89 Å) and the carbonyl oxygen of S196(191) (2.72 Å). HOH3 is located adjacent to HOH2 toward the cytoplasmic side and is hydrogen-bonded to the carbonyl oxygen of S197(192) (2.57 Å). The three water molecules are also hydrogen-bonded to each other, with HOH1 and HOH2 hydrogen-bonded to each other (2.5 Å), as are HOH2 and HOH3 (3.0 Å) (Fig. 2).

**Proteoliposome Swelling Assay.** After cleavage of the affinity tag, assays using purified AqpM reconstituted into liposomes reveal that it is active and functional in conductance of water (Fig. 4*A*). The curves represent the measured rate of vesicular shrinkage as a result of water efflux out of the proteoliposomes. This efflux is induced when vesicles are exposed to a sharp sucrose gradient (570 mM sucrose) in a stopped-flow light scattering measurement. The curves are fitted with a single exponential function as described by Borgnia and Agre (9), and the results indicate water permeability ($P_f$) of $60.5 \pm 3$ μm/s, comparable to that observed by Kozono *et al.* (13) using samples with the affinity tag still present on the samples. Our results show that the presence or absence of the affinity tag does not affect the water-conductance activity of AqpM.

## Discussion

**Water Conductance and Channel Architecture.** The presence of only water molecules at the selectivity filter correlates with the biophysical characterization of AqpM with preferential selection for water over glycerol. The two water molecules coordinated at the selectivity filter (HOH1 and HOH2) are both hydrogen-bonded to R202(206) and the main-chain carbonyl oxygens of S196(191) and G195(190), respectively (Fig. 2). When visualized in space filling representation (Fig. 3*A*), the selectivity filter is wide enough to accommodate the passage of water and highly restrictive toward the passage of glycerol. With some movement of the side chains, the channel may expand enough to allow the passage of glycerol, but the channel seen in this structure reveals why the rate of the passage of glycerol is very low when compared with the rate seen for the glycerol transporter GlpF. The high concentration of glycerol (10% vol/vol) in the crystallization condition accounts for its presence in the channel, but of all of the crystal structures of aquaporins (GlpF, Aqp1, AqpZ, and Aqp0), only that of the aquaglyceroporin GlpF has a glycerol molecule present in the selectivity filter (Fig. 3*D*). Also, despite the slight differences in the location of water and glycerol molecules in the channel between the high- and low-resolution structures, the location of two water molecules at the selectivity filter are identical between the two structures reported here. Therefore, the coordination of the water molecule at the selectivity filter, despite the presence of glycerol molecules at other regions of the channel, and the restrictive diameter of the channel represents a steric and electrostatic environment that is clearly adapted for the stabilization of water or chemically similar molecules at this site.

Based on amino acid sequence variations, structures, and permeation studies, the aquaporins can be classified into two distinct subfamilies, water-selective and glycerol-selective. The structure and sequence of AqpM positions it in a unique place between these two classes and establishes a paradigm applicable for the archaeal aquaporins. The substitution of the highly conserved histidine residue [H182(191) in bAQP1, H174(191) in AqpZ] in the selectivity filter of AqpM with an aliphatic I187(191) is a feature seen only in the archaeal aquaporins [I188(191) in *Archaeoglobales fulgidus* aquaporin, V186(191) in *Methanosarcina barkeri* aquaporin), I181(191) in *Methanococcus maripaludis*, and L218(191) in *Sulfolobus acidocaldarius*] (Fig.
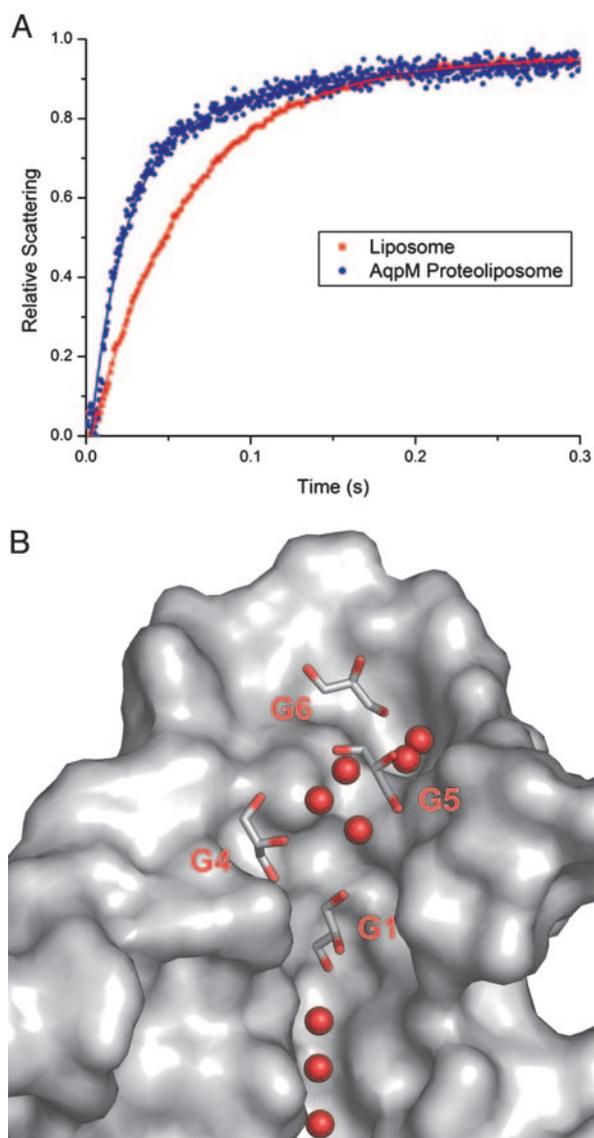
**BIOPHYSICS**

**Fig. 4.** Water conductance by AqpM and water and glycerol in the vestibule of the channel. (*A*) Water permeability of liposome-reconstituted AqpM. Liposomes reconstituted with purified AqpM or control liposomes were mixed at 12.2°C with an equal volume of hyperosmolar solution (570 mM sucrose). The reduction in vesicular volume caused by water efflux, resulting in an increase in light scattering, was observed in a stopped-flow apparatus for 0.5 s. The data were normalized between zero and unity and fitted to an exponential rise to the maximal value curve. Osmotic water permeabilities constants were calculated as follows: $P_f$(liposomes) = 15.5 ± 0.7 $\mu$m/s, $P_f$(AqpM proteoliposomes) = 60.5 ± 3 $\mu$m/s. (*B*) Shown is the surface rendering of AqpM with helices 3, 4, 7, and 8 removed to highlight the channel and vestibule. Three glycerol (G4–G6) and five water molecules can be seen in the pocket of the vestibule on the extracellular side of the channel. With its hydrophobic backbone facing the greasy portion of the channel, G4 is approximately in the optimal orientation before entering the narrow portion of the channel.

3*B*). Although this is only a single residue difference, this histidine residue is a highly conserved feature of water-selective aquaporins and represents one of the key distinctions between the two major subfamilies. In other respects, the selectivity filter of AqpM resembles that of the water-selective aquaporins. Two the four residues at the selectivity filter of AqpM, R202(206) and F62(48), match those of the water-selective Aqp1 and AqpZ, and these residues are seen in most of the water-selective subfamily. The third corner in the selectivity filter is the main-chain

carbonyl oxygen of S196(200), which displays an electrostatic environment that is essentially equivalent to that of the carbonyl oxygen of C191(200) of Aqp1 (Fig. 3*A*). However, the histidine-to-isoleucine substitution results in increases in both the cross-sectional surface area and the hydrophobicity of the selectivity filter of AqpM in comparison with Aqp1 or AqpZ. At the other end of the spectrum, the aquaglyceroporin GlpF has F200 and W48 opposite R206 in its selectivity filter, which is significantly more hydrophobic than the selectivity filter of AqpM (Fig. 3*D*). These differences in GlpF support a selectivity filter with a large hydrophobic surface thought to aid in the passage of glycerol by providing two hydrophobic planar walls, resembling the "greasy slide" as in maltoporin (21) for the carbon–hydrogen backbone of the glycerol molecule. Therefore, the unique occurrence of an aliphatic side chain at I187(191), with its structural consequences on the size and hydrophobicity of the key selectivity filter in AqpM, represents another subfamily among the aquaporins.

The structure of AqpM reinforces the importance of the electrostatic environment and the physical size of the selectivity filter in influencing the rate of water conductance through the aquaporin channel. The aquaporin channel structures, including that of AqpM, present the paradox that an increase in the cross-sectional surface area of the selectivity filter results in a decrease in the conductance rate for water. To date, the largest selectivity filter has been seen in the relatively poor water-conducting glycerol channel GlpF. In contrast, the much more efficient water channels Aqp1 and AqpZ display the most constricted selectivity filters. These observations suggest that channel diameter and charge distribution and hydrophobicity all play a part in the mechanism of selectivity and conductance rates for aquaporins. The size of the selectivity filter of AqpM is inhibitory toward the conductance of glycerol because of steric hindrance. On the other hand, it is reasonable to conclude that the larger channel diameter of AqpM in comparison with that of Aqp1 or AqpZ results in its relatively low conductance rate of water because of the exchange of the histidine with the aliphatic isoleucine residue at the selectivity filter and the resulting loss of a hydrogen-bonding partner at this crucial location in the channel.

**The Vestibules.** In addition to the water and glycerol molecules coordinated in the narrow pore of the channel, a network of water and glycerol molecules on the extracellular vestibule (Fig. 4*B*) form a contiguous chain of hydrogen-bonded molecules that extend from the surface of the protein into the narrow portion of the channel. The glycerol molecules seen in this pocket are oriented with their greasy backbone to the hydrophobic floor of this pocket and their OH groups hydrogen-bonded to water molecules or polar atoms along the walls of the pocket. The alignment of the hydrophobic wall of the narrow channel, matched by the hydrophobic backbone of glycerol in the structure, may equally serve to recruit other hydrophobic nutrients before entering the narrow portion of the channel.

The coordination of glycerol and water molecules in the pocket of the extracellular vestibule of AqpM indicates that the selectivity and conductance of permeant molecules begins in the vestibule of the channel. The energetically unfavorable process of shedding the hydration shell of water around the permeant is initiated in the vestibule as it transitions into the channel by hydrogen-bonding interaction with waters already in the pocket. Because the hydration shell is partially stripped before the permeant enters the narrow portion of the channel, transit through the channel might thus be expedited by this role of this unique vestibule. In addition to shedding the hydration shell of the waters, the vestibule may serve to increase the local concentration of waters at the mouth of the channel, effectively increasing the gradient and therefore the rate of water conductance through the channel.

**Thermo and pH Stability.** It is thought that membrane proteins of thermophilic organisms may be stabilized by properties of the interactions with their often very different lipids. For example, some lipids in archaea are double-headed, span the entire bilayer, and provide greater stability to the lipid bilayer. In the case of AqpM, we find that the pH and temperature stabilities are not a consequence of the lipids *per se*, but intrinsic to the purified protein alone. The unusual stability of detergent-purified AqpM was seen through its ability to maintain activity despite exposure to extreme pH (pH <4.2), temperatures ($T$ >80°C), and its resistance to dissociation from its biologically active tetrameric state into monomers even in 14% SDS/PAGE gels (13).

This stability is especially significant when compared with that of detergent-purified GlpF, which readily dissociates into monomers in solution (22, 23). The source of the stability of the tetramer of AqpM correlates with the higher surface area of interaction at the interface between the monomers when compared with other aquaporin structures. The surface area buried between two AqpM monomers totals 3,629 Å$^2$ and is greater than that calculated from other aquaporin structures to date (AqpZ = 3,340 Å$^2$, Aqp1 = 3,180 Å$^2$, GlpF = 3,060 Å$^2$). When these numbers are amplified 4-fold to account for the total surface area of interaction in the tetramer, the difference between AqpM and GlpF is a significant 2,276 Å$^2$. The increased interaction between monomers in AqpM has a major contribution from the unusually long helix M1 and loop A (residues 33–51) of AqpM versus other aquaporins. Notably, GlpF displays the smallest surface area of interaction and exhibits the highest propensity to dissociate into monomers among the aquaporins whose structures have been solved to date.

**Selectivity Filter and Rate of Conductance.** The structure of AqpM reveals a selectivity filter that is well structured to accommodate the passage of H$_2$O, but not as efficiently as the water-selective aquaporins such as Aqp1. The selectivity filter of Aqp1 coordi-nates the passing water molecule with the hydrogen-bond donors N$\varepsilon$ of R197(206) and the carbonyl oxygen of C191(200). H182(191) also facilitates the passage of the polar water molecule by providing a secondary hydrogen-bond partner for the passing H$_2$O molecule. The presence of histidine residue, located opposite the channel from the arginine residue, in Aqp1 facilitates the hydrogen-bonding requirements of a polar water molecule. The presence of the aliphatic I187(191) in AqpM, instead of a histidine residue, tunes the selectivity filter of AqpM for less efficient passage of H$_2$O, when compared with Aqp1.

The substitution of the highly conserved histidine with an isoleucine (I187) at the selectivity filter of AqpM suggests an adaptation for the conductance of larger and less polar permeant than water. This change in AqpM generates a selectivity filter that is wider and more hydrophobic (2.54 Å) than that of Aqp1 (1.86 Å). One can rule out glycerol as a possible permeant of AqpM because *Methanothermobacter marburgensis* uses CO$_2$ as its sole carbon source (24). This difference in hydrophobicity and size of the channel at the selectivity filter leads to the speculation that the differences in AqpM enables it to function as a multi-functional channel that conducts either H$_2$S or CO$_2$ in addition to water. *Methanothermobacter marburgensis* relies on H$_2$S as the terminal electron acceptor in its energy production pathway, and because of structural similarity of H$_2$S to H$_2$O, the mechanism of selectivity for these molecules must necessarily be very similar and leads to H$_2$S as a possible candidate for conductance by AqpM. It remains to be tested whether AqpM is indeed a novel member of the subclass of gas-conducting aquaporins.

1. Preston, G. M., Carroll, T. P., Guggino, W. B. & Agre, P. (1992) *Science* **256,** 385–387.
2. Fu, D., Libson, A., Miercke, L. J., Weitzman, C., Nollert, P., Krucinski, J. & Stroud, R. M. (2000) *Science* **290,** 481–486.
3. Murata, K., Mitsuoka, K., Hirai, T., Walz, T., Agre, P., Heymann, J. B., Engel, A. & Fujiyoshi, Y. (2000) *Nature* **407,** 599–605.
4. Sui, H., Han, B. G., Lee, J. K., Walian, P. & Jap, B. K. (2001) *Nature* **414,** 872–878.
5. Savage, D. F., Egea, P. F., Robles-Colmenares, Y., O'Connell, J. D., 3rd & Stroud, R. M. (2003) *PloS Biol.* **1,** 334–340.
6. Harries, W. E., Akhavan, D., Miercke, L. J., Khademi, S. & Stroud, R. M. (2004) *Proc. Natl. Acad. Sci. USA* **101,** 14045–14050.
7. Gonen, T., Sliz, P., Kistler, J., Cheng, Y. & Walz, T. (2004) *Nature* **429,** 193–197.
8. Borgnia, M. J., Kozono, D., Calamita, G., Maloney, P. C. & Agre, P. (1999) *J. Mol. Biol.* **291,** 1169–1179.
9. Borgnia, M. J. & Agre, P. (2001) *Proc. Natl. Acad. Sci. USA* **98,** 2888–2893.
10. Uehlein, N., Lovisolo, C., Siefritz, F. & Kaldenhoff, R. (2003) *Nature* **425,** 734–737.
11. Ding, X. & Kitagawa, Y. (2001) *J. Biosci. Bioeng.* **92,** 488–491.
12. Roberts, M. F. (2000) *Front. Biosci.* **5,** D796–D812.
13. Kozono, D., Ding, X., Iwasaki, I., Meng, X., Kamagata, Y., Agre, P. & Kitagawa, Y. (2003) *J. Biol. Chem.* **278,** 10649–10656.
14. Yang, B., Fukuda, N., van Hoek, A., Matthay, M. A., Ma, T. & Verkman, A. S. (2000) *J. Biol. Chem.* **275,** 2686–2692.
15. Verkman, A. S. (2002) *J. Physiol. (London)* **542,** 31.
16. Prasad, G. V., Coury, L. A., Finn, F. & Zeidel, M. L. (1998) *J. Biol. Chem.* **273,** 33123–33126.
17. Otwinowski, Z. & Minor, W. (1997) *Methods Enzymol.* **276,** 307–326.
18. Brunger, A. T., Adams, P. D., Clore, G. M., DeLano, W. L., Gros, P., Grosse-Kunstleve, R. W., Jiang, J. S., Kuszewski, J., Nilges, M., Pannu, N. S., *et al.* (1998) *Acta Crystallogr. D* **54,** 905–921.
19. Gerber, P. R. & Muller, K. (1995) *J. Comput. Aided Mol. Des.* **9,** 251–268.
20. Smart, O. S., Goodfellow, J. M. & Wallace, B. A. (1993) *Biophys. J.* **65,** 2455–2460.
21. Van Gelder, P., Dumas, F., Bartoldus, I., Saint, N., Prilipov, A., Winterhalter, M., Wang, Y., Philippsen, A., Rosenbusch, J. P. & Schirmer, T. (2002) *J. Bacteriol.* **184,** 2994–2999.
22. Lagree, V., Froger, A., Deschamps, S., Pellerin, I., Delamarche, C., Bonnec, G., Gouranton, J., Thomas, D. & Hubert, J. F. (1998) *J. Biol. Chem.* **273,** 33949–33953.
23. Bron, P., Lagree, V., Froger, A., Rolland, J. P., Hubert, J. F., Delamarche, C., Deschamps, S., Pellerin, I., Thomas, D. & Haase, W. (1999) *J. Struct. Biol.* **128,** 287–296.
24. Smith, D. R., Doucette-Stamm, L. A., Deloughery, C., Lee, H., Dubois, J., Aldredge, T., Bashirzadeh, R., Blakely, D., Cook, R., Gilbert, K., *et al.* (1997) *J. Bacteriol.* **179,** 7135–7155.
25. Kraulis, P. (1991) *J. Appl. Crystallogr.* **24,** 946–950.
26. Merritt, E. & Bacon, D. (1997) *Methods Enzymol.* **277,** 505–524.
27. DeLano, W. L. (2002) PYMOL: *The Molecular Graphics System* (DeLano Scientific, South San Francisco).

**BIOPHYSICS**